

# Baryon Rapidity Loss in Relativistic Au+Au Collisions

B.B. Back,<sup>1</sup> R.R. Betts,<sup>1,5</sup> J. Chang,<sup>3</sup> W.C. Chang,<sup>3,\*</sup> C.Y. Chi,<sup>4</sup> Y.Y. Chu,<sup>2</sup>  
 J.B. Cumming,<sup>2</sup> J.C. Dunlop,<sup>7,†</sup> W. Eldredge,<sup>3</sup> S.Y. Fung,<sup>3</sup> R. Ganz,<sup>5,‡</sup> E. Garcia-Solis,<sup>6</sup>  
 A. Gillitzer,<sup>1,§</sup> G. Heintzelman,<sup>7,\*\*</sup> W.F. Henning,<sup>1,††</sup> D.J. Hofman,<sup>1,‡‡</sup> B. Holzman,<sup>5</sup>  
 J.H. Kang,<sup>9</sup> E.J. Kim,<sup>9</sup> S.Y. Kim,<sup>9</sup> Y. Kwon,<sup>9</sup> D. McLeod,<sup>5</sup> A.C. Mignerey,<sup>6</sup>  
 M. Moulson,<sup>4,§§</sup> V. Nanal,<sup>1,\*\*\*</sup> C.A. Ogilvie,<sup>7</sup> R. Pak,<sup>8</sup> A. Ruangma,<sup>6</sup> D.E. Russ,<sup>6</sup>  
 R.K. Seto,<sup>3</sup> P.J. Stankas,<sup>6</sup> G.S.F. Stephans,<sup>7</sup> H.Q. Wang,<sup>3</sup> F.L.H. Wolfs,<sup>8</sup>  
 A.H. Wuosmaa,<sup>1</sup> H. Xiang,<sup>3</sup> G.H. Xu,<sup>3,†††</sup> H.B. Yao,<sup>7</sup> and C.M. Zou<sup>3</sup>

(E917 Collaboration)

<sup>1</sup>*Argonne National Laboratory, Argonne, IL 60439, USA*

<sup>2</sup>*Brookhaven National Laboratory, Upton, NY 11973, USA*

<sup>3</sup>*University of California, Riverside, CA 92521, USA*

<sup>4</sup>*Columbia University, Nevis Laboratories, Irvington, NY 10533, USA*

<sup>5</sup>*University of Illinois at Chicago, Chicago, IL 60607, USA*

---

\*Institute of Physics, Academia Sinica, Taipei 11529, Taiwan

†Yale University, New Haven, CT 06520, USA

‡Max Planck Institut für Physik, D-80805 München, Germany

§Institut für Kernphysik, Forschungszentrum Jülich, D-52425 Jülich, Germany

\*\*Brookhaven National Laboratory, Upton, NY 11973, USA

††Gesellschaft für Schwerionenforschung, D-64291 Darmstadt, Germany

‡‡University of Illinois at Chicago, Chicago, IL 60607, USA

§§Laboratori Nazionali di Frascati, INFN, 00044 Frascati, Italy

\*\*\*Tata Institute of Fundamental Research, Colaba, Mumbai 400005, India

†††University of Houston, Houston, TX 77004, USA

<sup>6</sup>*University of Maryland, College Park, MD 20742, USA*

<sup>7</sup>*Massachusetts Institute of Technology, Cambridge, MA 02139, USA*

<sup>8</sup>*University of Rochester, Rochester, NY 14627, USA*

<sup>9</sup>*Yonsei University, Seoul 120-749, South Korea*

## Abstract

An excitation function of proton rapidity distributions for different centralities is reported from AGS Experiment E917 for Au+Au collisions at 6, 8, and 10.8 GeV/nucleon. The rapidity distributions from peripheral collisions have a valley at midrapidity which smoothly change to distributions that peak at midrapidity for central collisions. The mean rapidity loss increases with increasing beam energy, whereas the fraction of protons consistent with isotropic emission from a thermal source at midrapidity decreases with increasing beam energy.

PACS number(s): 25.75.-q, 13.85.Ni, 21.65.+f

Nuclear matter is compressed to high baryon density  $\rho_B$  during central collisions of heavy nuclei at relativistic energies [1–3]. In the interaction region of the colliding nuclei, nucleons suffer collisions which reduce their original longitudinal momentum. This rapidity loss is an important characteristic of the reaction mechanism, and is often referred to as stopping [4]. The loss of rapidity for beam nucleons has been extensively studied in p+A reactions [5] and more recently in heavy-ion reactions [6–9]. Relativistic heavy-ion collisions are unique in the sense that secondary collisions of highly excited baryons are expected to contribute to the rapidity loss leading to simultaneous stopping of many nucleons within the interaction volume. The  $\rho_B$  achieved may be large enough to induce phase transitions, such as quark deconfinement and/or chiral symmetry restoration. The observation of baryon pile-up at midrapidity is indicative of compression to high  $\rho_B$ , but the link between these quantities is only possible via model calculations. Key to our understanding of heavy-ion collisions is the measurement of the rapidity distribution of baryons over a broad range of conditions, *i.e.*, as a function of the beam energy and centrality.

In this Letter, we present an excitation function of the centrality dependence of proton rapidity distributions from Au+Au collisions at 6, 8, and 10.8 GeV/nucleon. At these energies, the ratio of antiprotons to protons is negligible [10] and the production of protons from  $\Lambda$  decay contributes less than 5% to the total yield [11], so that protons can be considered a probe that directly reflects the baryon rapidity loss. To further our understanding of the reaction mechanism independent of detailed transport models, several derived quantities are calculated from the measured proton rapidity distributions. The mean rapidity loss characterizes the average rapidity shift with respect to the incident beam. However, these protons do not necessarily end up in an isotropically emitting source at midrapidity, but often retain a fair degree of longitudinal motion. This phenomenon is represented by a parameterized fit to the data with a superposition of longitudinally moving sources.

Experiment E917 measured Au+Au reactions at beam kinetic energies of 6, 8, and 10.8 GeV/nucleon at the Brookhaven AGS, and was the final experiment in the series E802/E859/E866/E917 [12,13]. The experimental apparatus in E917 consisted of a series

of beamline detector arrays, used for global event characterization, and a large rotatable magnetic spectrometer, used to track and identify particles. The tracking system of the spectrometer consists of a series of drift and multiwire ionization chambers which bracket either side of the Henry Higgins dipole magnet, followed by a segmented time-of-flight wall of vertical scintillator slats. The data presented here were taken with a trigger that required at least one track in the spectrometer. The centrality of an event can be selected through either of two equivalent methods: (1) from the multiplicity measured by a large acceptance device called the New Multiplicity Array [14], or (2) from the energy deposited in the zero degree calorimeter [14]. The data were sorted off-line into different centrality classes, where normalization was provided by prescaled interaction triggers. For each beam energy, the five event classes are reported as the percentage of the total inelastic cross section ( $\sigma_{\text{int}} = 6.8 \text{ b}$ ). These centrality cuts correspond to (0-5)%, (5-12)%, (12-23)%, (23-39)%, and (39-81)% ((39-77)% for 10.8 GeV/nucleon) of  $\sigma_{\text{int}}$ . The systematic uncertainty on the normalization of the measured invariant spectra and rapidity distributions is dominated by the uncertainty of the single-track efficiency and the loss of tracks due to hit-blocking. The tracking uncertainty increases from 5% to 10% the closer to midrapidity and the more central the event class. For peripheral collisions, there is a 10% uncertainty in the cross section, which decreases to 5% for central collisions. These uncertainties lead to a total systematic uncertainty of 15% independent of centrality, with a 5% relative uncertainty across beam energies.

Measured invariant proton yields from Au+Au collisions at 8 GeV/nucleon, divided by the reaction cross section for the event class, are shown in Fig. 1 plotted as a function of transverse mass in ten different rapidity intervals. The transverse mass is defined as  $m_t = \sqrt{p_t^2 + m_0^2}$ , where  $p_t$  is the transverse momentum and  $m_0$  is the rest mass of the proton. The data for laboratory rapidity  $0.5 < y < 0.6$  are plotted to scale while, for clarity, each successive spectrum is divided by an additional factor of ten for each rapidity slice. These spectra are representative of the quality of the data at the other beam energies. The error bars are statistical only, and are either shown or are smaller than the size of the data

point.

Each spectrum in Fig. 1 was fit with the following Boltzmann-form function in  $m_t$ :

$$\frac{1}{2\pi m_t} \frac{d^2 N}{dm_t dy} = \frac{dN/dy}{2\pi(m_0^2 T + 2m_0 T^2 + 2T^3)} m_t e^{-(m_t - m_0)/T} \quad (1)$$

where  $T$  and  $dN/dy$  are free parameters. In these fits, the data points were weighted according to their statistical errors only. As previously reported for Au+Au collisions at 10.8 GeV/nucleon [3], the proton spectra cannot be satisfactorily described by a single exponential function. In contrast, the above form reproduces the spectra well, and provides the inverse slope parameter  $T$  and the rapidity density  $dN/dy$  in each rapidity slice. The spectra become flatter at all rapidities as the collisions become more central corresponding to an increase in the value of  $T$  obtained from the fits.

Figure 2 shows the centrality dependence for the rapidity density as a function of rapidity at each beam energy. The data are shown relative to the rapidity of the center-of-mass of the system  $y_{\text{cm}}$  which is 1.346, 1.474, and 1.613 for beam kinetic energies of 6, 8, and 10.8 GeV/nucleon, respectively. The open symbols are the data points reflected about midrapidity. The error bars shown in Fig. 2 are statistical only, and were obtained by varying  $\chi^2$  around its minimum. The present values of  $dN/dy$  for the most central event class at 10.8 GeV/nucleon are in agreement with the values previously reported by the E866 Collaboration [3].

For each beam energy, a common trend is observed for the evolution of the shape of the rapidity distributions as a function of centrality. For the most peripheral event class the distribution has a minimum value of  $dN/dy \approx 6$  at midrapidity. This bowl-like shape persists to the next most central event class corresponding to a centrality cut of (23-39)%. The shape of the rapidity distributions for these two event classes is consistent with the expectation that most of the protons are at spectator rapidities following these relatively peripheral collisions. The rapidity distributions become progressively flatter, and begin to develop a maximum at midrapidity for all beam energies, which is most pronounced for the distribution at 10.8 GeV/nucleon with a value of  $dN/dy \approx 65$ . The shape of the rapidity

distributions for the most central event class indicates that the protons have moved away from the spectator regions predominant in peripheral collisions to pile-up at midrapidity.

The shape of the proton rapidity distributions at 10.8 GeV/nucleon changes more rapidly with centrality than at 6 and 8 GeV/nucleon, implying that protons from 10.8 GeV/nucleon reactions lose more rapidity than at the lower beam energies for central reactions. This observation can be quantified by calculating the mean rapidity loss for central collisions:

$$\langle \delta y \rangle = \frac{\sum \frac{dN}{dy} |y_{\text{beam}} - y|}{\sum \frac{dN}{dy}}, \quad (2)$$

according to the prescription outlined in Ref. [6], where the sum extends over the data points. The values of the mean rapidity loss  $\langle \delta y \rangle$  thus obtained at all three beam energies in the rapidity range  $0.5 < y < y_{\text{midrapidity}}$  are given in the second column of Table I. The 10.8 GeV/nucleon data have been extrapolated from the last measured point at  $y = 1.45$  to midrapidity at  $y = 1.61$  assuming a constant  $dN/dy$ . This analysis indicates that the mean rapidity loss increases as the beam energy increases over the measured range. There is agreement between  $\langle \delta y \rangle$  for the most central events at 10.8 GeV/nucleon and the value of  $1.02 \pm 0.01$  for the (0-4)% most central Au+Au collisions at the same beam energy from E866 previously reported by Videbæk and Hansen [6].

The mean rapidity loss calculated over the fiducial range does not fully characterize the shape of the final rapidity distribution. To gain more insight into the shape of the proton distributions a simple parameterization for the central data was developed. The experimental proton  $dN/dy$  distributions and inverse slopes for the (0-5)% most central event class at each beam energy are shown as solid points in Fig. 3 as a function of rapidity ( $y_{\text{cm}}$  is the rapidity of the center-of-mass of the system); open points are reflected around midrapidity. The solid curves in this figure represent the expected emission from a continuum of isotropic sources, which are uniformly distributed over a rapidity range  $y_{\text{cm}} \pm y_b$ . Reproducing the measured dependence of the inverse slopes on rapidity (see Fig. 3(d-f)) required the introduction of a Gaussian dependence for the isotropic source inverse slope parameters, *i.e.*,  $T_{\text{eff}}(y) = T_{\text{eff}}^0 \exp(-(y - y_{\text{cm}})^2/2\sigma_T^2)$ . The solid curves shown in Fig. 3 are obtained by a

four parameter simultaneous fit of  $y_b$ ;  $T_{\text{eff}}^0$ ;  $\sigma_T$ ; and  $N_0$  ( $dN/dy$  normalization) to the experimental  $dN/dy$  and inverse slope  $T(y)$  values. As a cross check, the total number of protons ( $\int_{-2}^2 \frac{dN}{dy} dy$ ) was found to be 155, 164, and 159 for  $E_{\text{beam}} = 6, 8, \text{ and } 10.8$  GeV/nucleon, respectively.

The resulting values for the absolute rapidity loss  $\langle \delta y \rangle_{\text{ext}}$  are listed in column 4 of Table I. The rapidity losses, scaled by the maximum possible value, *i.e.*,  $y_{\text{max}} = y_{\text{beam}} - y_{\text{cm}}$ , are listed in columns 3 and 5. The absolute rapidity losses  $\langle \delta y \rangle$  and  $\langle \delta y \rangle_{\text{ext}}$  increase with beam energy. This result is different from what was observed in p+A reactions where the rapidity loss was found to be independent of beam energy [5], potentially indicating the role of secondary collisions in increasing the stopping in heavy-ion reactions. The fractional rapidity loss  $\langle \delta y \rangle_{\text{ext}} / \delta y_{\text{max}}$  obtained from the fully extrapolated  $dN/dy$  distributions (column 5, Table I) are almost constant with beam energy from 6 to 158 GeV/nucleon, similar to the trend found in Ref [8].

This parameterization indicates that there is substantial longitudinal motion in the final state and that the protons cannot be considered as emitted from a stationary source centered at midrapidity. The dashed curves in Fig. 3 represent the expected rapidity and inverse slope distributions for isotropic emission from a single source at rest in the c.m. frame. The inverse slope parameter  $T_{\text{eff}}$  of this source was adjusted to reproduce the observed inverse slope distribution, resulting in values of  $T_{\text{eff}} = 0.208, 0.220, \text{ and } 0.235$  GeV/ $c^2$  for the 6, 8, and 10.8 GeV/nucleon data, respectively. The overall normalization has been adjusted to account for the observed values of  $dN/dy$  at midrapidity. One measure of how the longitudinal motion varies with beam energy is to calculate the fraction of nucleons  $f_{\text{iso}}$  contained within the dashed line compared to the solid line in Fig. 3. This is the maximum number of nucleons that could be considered as coming from a completely stopped isotropic source centered at midrapidity. We observe that the fraction of isotropically emitted protons  $f_{\text{iso}}$  decreases with beam energy over the range of the present study, and that this trend is continued to SPS energies (see last column Table I). This observation indicates that longitudinal motion of the protons increases in importance as the beam energy increases, such that a smaller

fraction of the protons in the entrance channel experience total rapidity loss.

In conclusion, the change in the shape of the proton  $dN/dy$  distributions with event centrality indicates large baryon rapidity loss during the most central Au+Au collisions. This observation provides additional evidence for the formation of a state with  $\rho_B$  substantially greater than for normal nuclear matter. The two key results presented in this Letter are that the mean rapidity loss increases with beam energy, and that the shape of the rapidity distribution changes more rapidly with centrality at the higher beam energies. Both observations suggest that secondary collisions play a larger role in rapidity loss as the beam energy increases. The data are not in agreement with the formation and decay of an equilibrated thermal source following complete stopping. Rather, there is significant longitudinal motion even in the most central collisions at all three beam energies.

The authors would like to acknowledge interesting discussions with Wit Busza. This work is supported by the U.S. Department of Energy under contracts with ANL (No. W-31-109-ENG-38), BNL (No. DE-AC02-98CH10886), MIT (No. DE-AC02-76ER03069), UC Riverside (No. DE-FG03-86ER40271), UIC (No. DE-FG02-94ER40865), and the University of Maryland (No. DE-FG02-93ER40802), the National Science Foundation under contract with the University of Rochester (No. PHY-9722606), and the Ministry of Education and KOSEF (No. 951-0202-032-2) in Korea.



## REFERENCES

- [1] L. Ahle *et al.*, Nucl. Phys. **A590**, 249c (1995).
- [2] L. Ahle *et al.*, Nucl. Phys. **A610**, 139c (1996).
- [3] L. Ahle *et al.*, Phys. Rev. C **57**, R466 (1998).
- [4] W. Busza and A.S. Goldhaber, Phys. Lett. **B139**, 235 (1984).
- [5] W. Busza and R. Ledoux, Ann. Rev. Nucl. Part. Sci. **38**, 119 (1988).
- [6] F. Videbæk and O. Hansen, Phys. Rev. C **52**, 2684 (1995).
- [7] J.W. Harris, in *Advances in Nuclear Dynamics 2*, Eds. Bauer and Westfall, Plenum Press, NY, (1996).
- [8] B. Hong *et al.*, Phys. Rev. C **57**, 244 (1998).
- [9] H. Appelshäuser *et al.*, Phys. Rev. Lett. **82**, 2471 (1999).
- [10] G. Heintzelman, Ph.D. thesis, MIT (1999).
- [11] W. Eldredge, Ph.D. thesis, UC Riverside (2000).
- [12] T. Abbott *et al.*, Nucl. Instrum. Meth. **A290**, 41 (1990).
- [13] L. Ahle *et al.*, Phys. Rev. C **58**, 3523 (1998).
- [14] L. Ahle *et al.*, Phys. Rev. C **59**, 2173 (1999).

# FIGURES

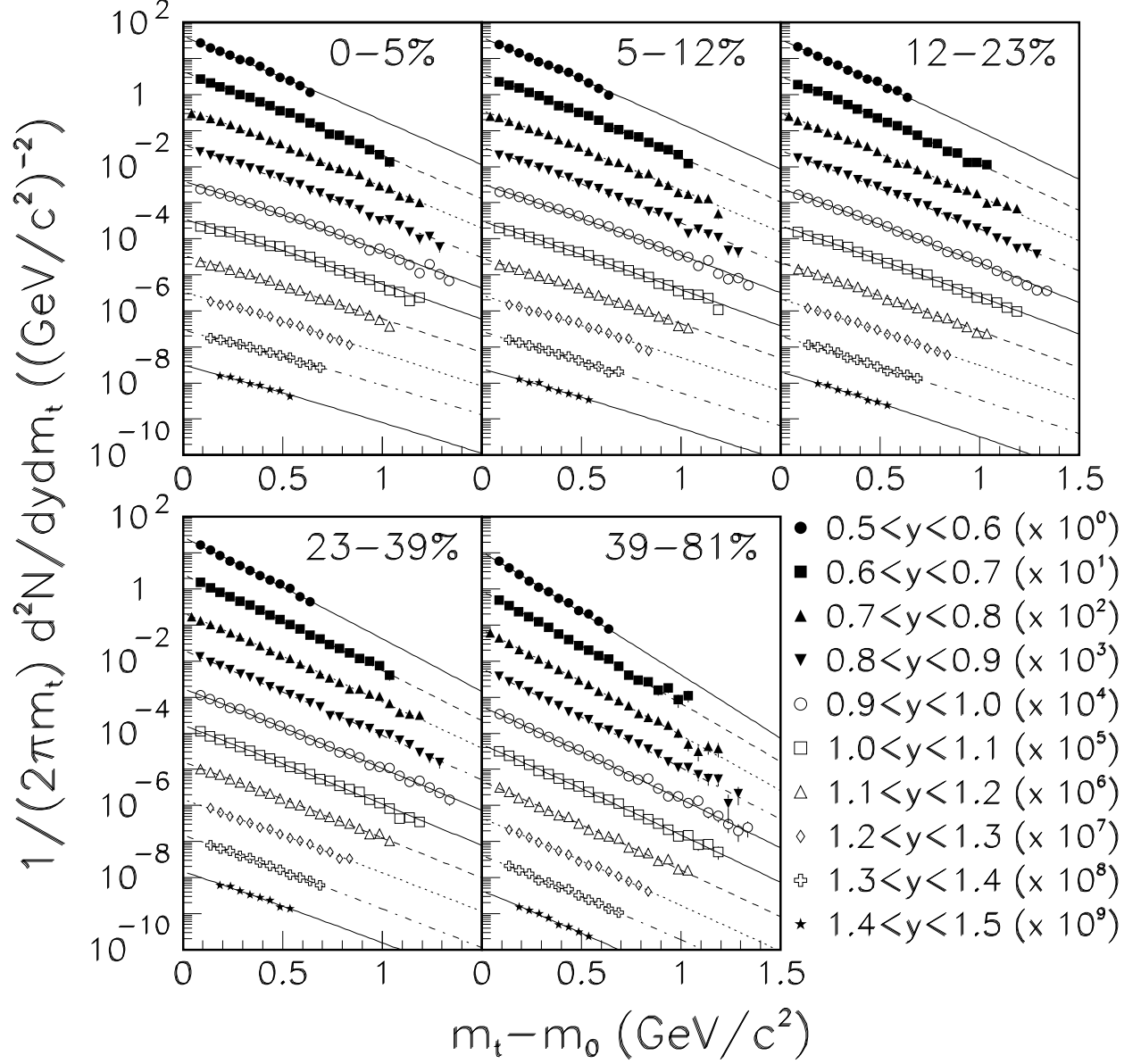


FIG. 1. Invariant yield of protons as a function of transverse mass for ten different rapidity slices for each centrality class of Au+Au collisions at 8 GeV/nucleon. The most backward rapidity in each panel is plotted on the correct scale, while successive spectra have been divided by ten for clarity. The errors are statistical only. The lines are Boltzmann fits described in the text.

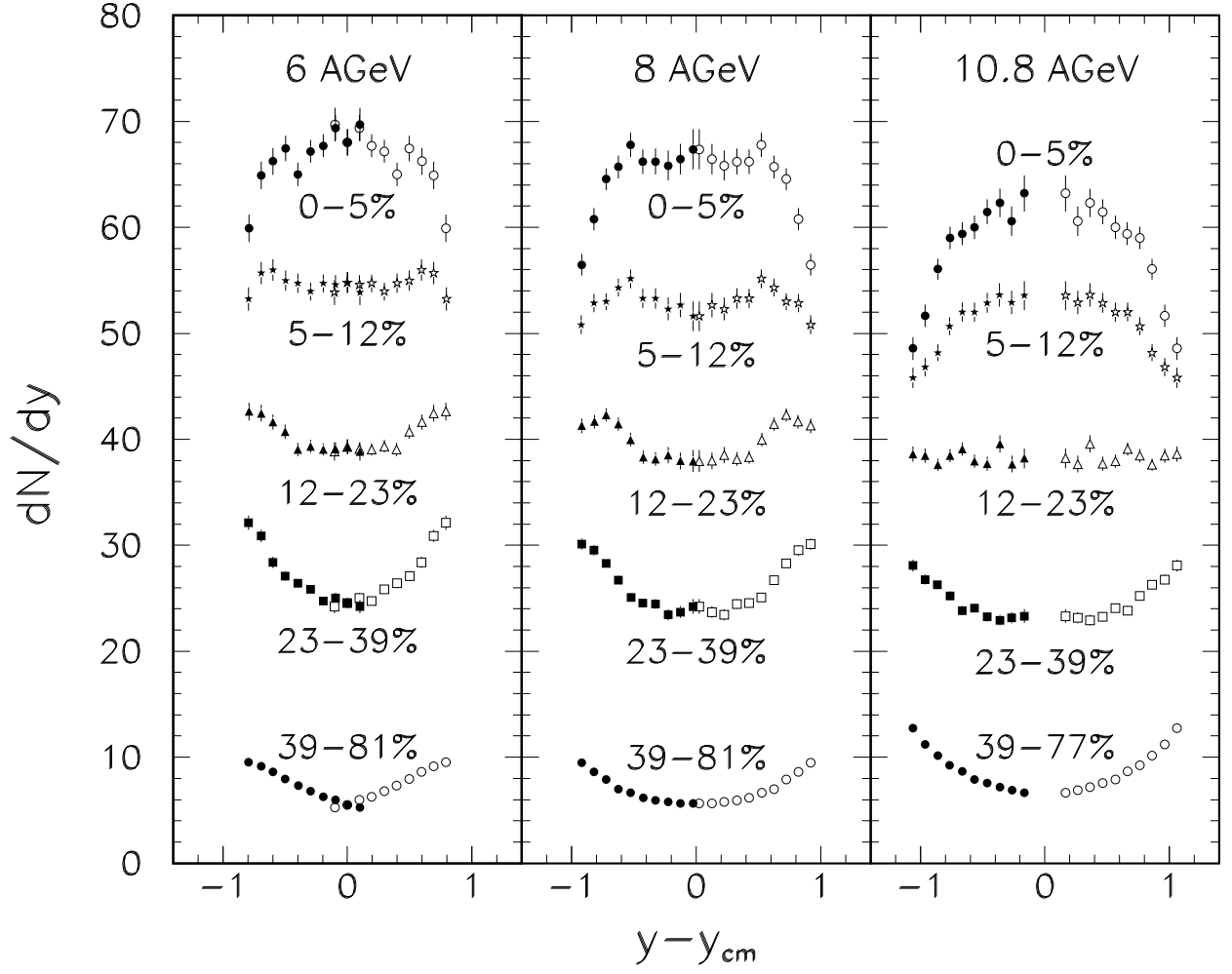


FIG. 2. Proton rapidity distributions for all centrality classes at all three beam energies from Boltzmann fits to the invariant cross sections. The open symbols are the data reflected about midrapidity. The errors are statistical only.

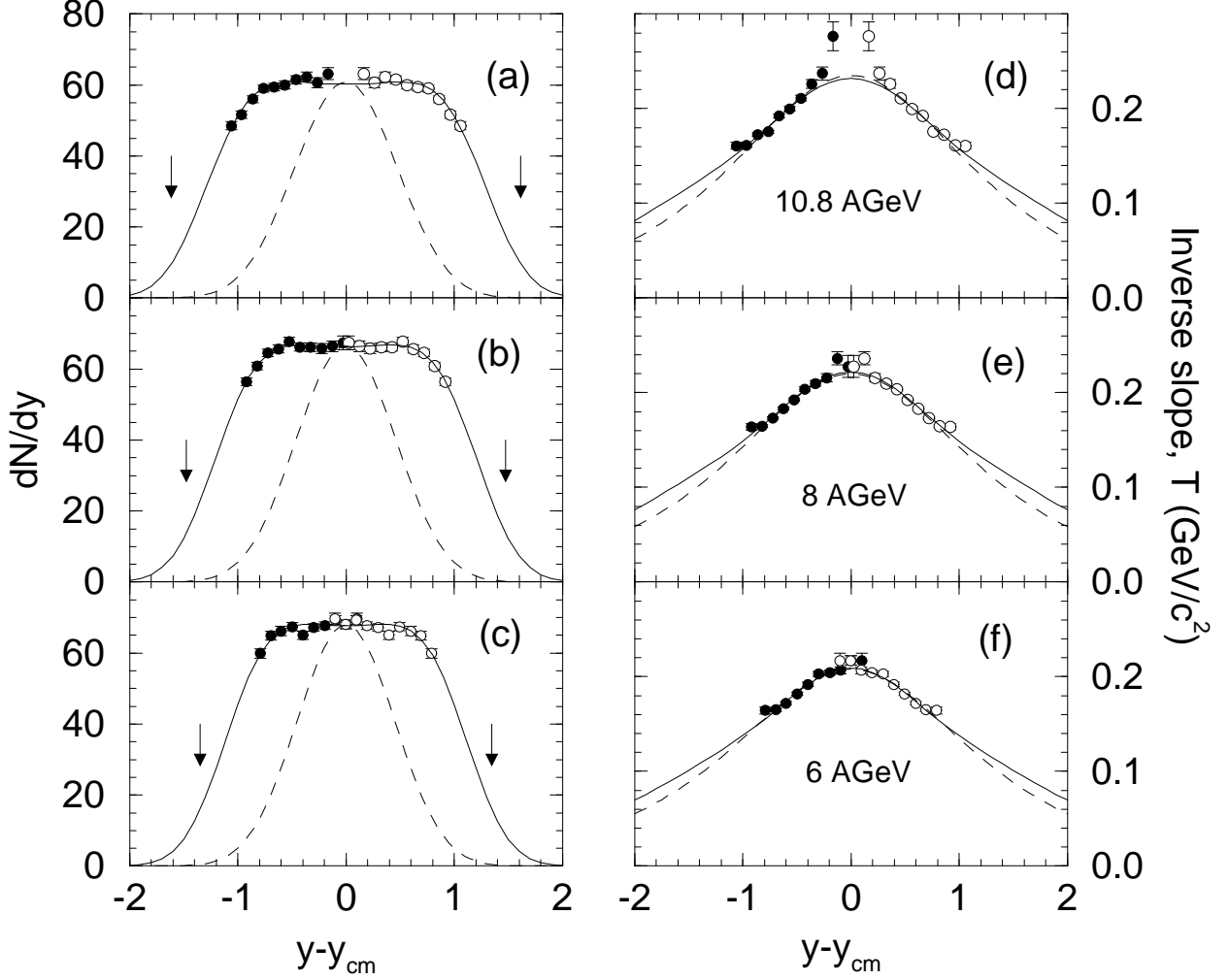


FIG. 3. Measured (solid points) and reflected (open circles) proton rapidity distributions and inverse slopes are shown as a function of rapidity  $y - y_{cm}$  for beam energies of 6, 8, and 10.8 GeV/nucleon. The arrows indicate the target and beam rapidities. The dashed curves represent the expected distribution for isotropic emission from a thermal source at rest in the center-of-mass system ( $y = y_{cm}$ ), whereas the solid curves correspond to an optimum fit to the data for a uniform distribution of sources within a range of rapidities  $(y_{cm} - y_b) < y < (y_{cm} + y_b)$  with a Gaussian profile of  $T_{\text{eff}}(y)$  centered at  $y_{cm}$  (see text). The parameters obtained from a least squares fit to the data are  $y_b = 0.990, 1.086, 1.166$ ,  $T_{\text{eff}}^0 = 0.253, 0.267, 0.279 \text{ GeV}/c^2$ , and  $\sigma_T = 0.697, 0.762, 0.809$  for  $E_{\text{beam}} = 6, 8, 10.8 \text{ GeV/nucleon}$ , respectively.

# TABLES

TABLE I. Comparison between different measures of stopping in central heavy-ion collisions. The absolute  $\langle\delta y\rangle$  and relative  $\langle\delta y\rangle/\delta y_{\text{max}}$  rapidity losses obtained from the measured data over the rapidity range  $0.5 < y < y_{\text{cm}}$  are given in column 2 and 3, respectively. The absolute and relative rapidity losses obtained from the fitted solid curves in Fig. 3(a-c) are given in column 4 and 5, respectively. Upper limits on the isotropic fraction  $f_{\text{iso}}$  of the total  $dN/dy$  distribution (solid curves in Fig. 3(a-c)) are given in column 6.

$E_{\text{beam}}$	$0.5 < y < y_{\text{cm}}$		$-\infty < y < y_{\text{cm}}$		$f_{\text{iso}}^{(a)}$
(AGeV)	$\langle\delta y\rangle$	$\langle\delta y\rangle/\delta y_{\text{max}}$	$\langle\delta y\rangle_{\text{ext}}^{(b)}$	$\langle\delta y\rangle_{\text{ext}}/\delta y_{\text{max}}^{(b)}$	
6.0	$0.96\pm 0.04$	$0.71\pm 0.03$	$0.74\pm 0.01$	$0.55\pm 0.01$	$0.49\pm 0.01$
8.0	$1.01\pm 0.04$	$0.69\pm 0.04$	$0.82\pm 0.01$	$0.56\pm 0.01$	$0.46\pm 0.01$
10.8	$1.07\pm 0.05$	$0.66\pm 0.05$	$0.93\pm 0.01$	$0.57\pm 0.01$	$0.45\pm 0.01$
158	$1.76\pm 0.05^{(c)}$	$0.61\pm 0.02$	$1.68\pm 0.02^{(d)}$	$0.58\pm 0.01$	$0.23\pm 0.02^{(e)}$

<sup>a</sup>Fraction of isotropically emitted proton (dashed curves in Fig. 3(a-c)) of total number of protons (solid curves of Fig. 3(a-c)).

<sup>b</sup>Statistical errors only.

<sup>c</sup>Taken from [9].

<sup>d</sup>Obtained from a double Gaussian fit,  $dN/dy = 85[\exp(-(y-y_{\text{cm}}+1.19)^2/1.6) + \exp(-(y-y_{\text{cm}}-1.19)^2/1.6)]$  to the experimental data.

<sup>e</sup>Obtained using  $T_{\text{iso}} = 0.26 \text{ GeV}/c^2$ , which reproduces  $\langle p_t \rangle$  at  $y - y_{\text{cm}} = 0$ .